Hindawi
Advances in Civil Engineering
Volume 2020, Article ID 7945135, 15 pages
https://doi.org/10.1155/2020/7945135

Research Article

Dynamic Response of a Casting Crane Rigid-Flexible Coupling System to High Temperature

Yunsheng Xin, Qing Dong, Qisong Qi, and Qinglu Shi

School of Mechanical Engineering, Taiyuan University of Science and Technology, Taiyuan 030024, China

Correspondence should be addressed to Qinglu Shi; shiqinglu@tyust.edu.cn

Received 6 August 2019; Revised 18 November 2019; Accepted 7 December 2019; Published 9 January 2020

Academic Editor: Melina Bosco

Copyright © 2020 Yunsheng Xin et al. This is an open access article distributed under the Creative Commons Attribution License, which permits unrestricted use, distribution, and reproduction in any medium, provided the original work is properly cited.

To determine the influence of temperature on the mechanical properties of crane metal structures, three Q355 alloy steel samples were processed and their elastic moduli were tested at different temperatures using a metal tension test bed. The constitutive equation for the elastic modulus of Q355 alloy steel at different temperatures was predicted using test data and a neural network algorithm. Based on crane structural characteristics and the principle of system dynamics, a coupling vibration model was established that included the crane flexible girder, cabin, trolley, crane, and temperature. System motion equations were established according to the Lagrange equation, and the approximate solution of nonlinear system vibration was solved by the direct integration method (the Newmark method). The dynamic characteristics of the main beam and cabin were analyzed at different temperatures, as well as safety during service. The results show that, with increasing temperature, the maximum midspan displacement of the main beam increases gradually, by 14.3%, 21.4%, and 57.1% at temperatures of 300°C, 400°C, and 600°C, respectively. The cabin vibration displacement increases with temperature, by up to 32.5% at 600°C, but the influence of temperature on cabin vibration acceleration is not obvious. It was concluded that the influence of temperature on the dynamic characteristics of the main beam must be considered during the design stage of cranes. The proposed model and analysis method provide a theoretical basis for the design of casting cranes according to temperature.

1. Introduction

Casting cranes are one of the most important devices in steelmaking and the continuous casting process and key heavy machinery equipment for mechanized and automated production [1]. They are predominantly used for loading and unloading molten steel in modern steel plants; thus, they operate in harsh environments characterized by high temperature and dust content. Because the temperature of the ladle is very high, approximately 1600°C, casting crane accidents can cause substantial losses to human life and wealth [2]; therefore, crane design standards are very high to ensure operational safety and reliability. The main beam of the crane close to the molten steel is subjected to intense thermal radiation, which results in a much higher temperature of the crossbeam than normal. Because the main body of the casting crane is a steel structure, the physical properties and mechanical properties of the material are sensitive to temperature, and its performance differs substantially between high and normal temperatures [3]. Moreover, the dynamic characteristics of the bridge structure are affected by many factors. Therefore, understanding the thermoelastic coupling dynamics of the main beam of a casting crane has important engineering applications.

In high-temperature environments, the mechanical properties of metal materials will change significantly, which can directly affect the structure's service life and safety performance of casting crane equipment. Therefore, many studies have investigated the mechanical properties of metal materials. Kirby and Preston [4] tested metal specimens under different loads at high temperature and recorded a series of strain-temperature curves and stress-strain curves for steel at different temperatures, ultimately deriving the relationship between the elastic modulus and temperature of steel. Cold-formed steels were studied by Chen and Young [5]. Kodur et al. [6] reviewed high-temperature constitutive

relationships for standard steel currently available in America and Europe and highlighted the variation between these relationships through a comparison with published experimental results.

As for the mechanical properties of building steel structures in high-temperature environments, Lu and Zhu [7] analyzed the structural response of a reinforced concrete frame by the nonlinear finite element method according to simulation results, constitutive relationship experiments, unstable heat conduction theory, and the nonlinear direct stiffness method. Through experiments, Lv [8] analyzed the strength and deformation of building steel bars at different temperatures, including the strength, stress-strain curve, elastic modulus, deformation under stress, and short-term creep of all grades of steel bars in the range of 20–800°C. The strength of five grades of steel bars decreased continuously with increasing temperature. Short-term creep of a steel bar is larger than creep at normal temperature and tends to be unstable at higher temperature and stress. Tan [9] established and validated a theoretical model of yield strength, ultimate strength, elasticity modulus, and ultimate strain for the commonly used Q235 steel with temperature. Qiang et al. [10] conducted tensile tests and obtained the postfire elastic modulus, yield, ultimate strength, ductility, and stress-strain curves before proposing two separate sets of predictive equations for evaluating the mechanical properties of S460 and S690 steels after a fire. Wang et al. [11] proposed a new set of equations to predict the postfire mechanical properties of high-strength Q460 steel. Such postfire mechanical property assessments allow structural and fire engineers to make accurate predictions of the safety of high-strength Q460 steel buildings exposed to fire. Based on material properties generated from the research on the thermal and mechanical properties of steel at elevated temperatures, a number of code's specifications for fire-resistant design have been developed, such as EN1993-1-2 [12], AS4100 [13], ANSI/AISC360-05 [14], BS 5950-1:2000 [15], and GB 51249-2017 [16]. In line with the steady-state test results for high-tensile steels, the elastic modulus is similar in the codes.

In addition to the effect of temperature, the influence of wire rope vibration during ladle hoisting should be considered. Additionally, the dynamic characteristics of the main beam of the casting crane are influenced by many factors; for example, the installation position and connection parameters of the cabin will affect the main beam dynamic characteristics and the vibration comfort of the human body. In addition, operation of the trolley has an impact on the deflection of the main beam, which will increase under increased temperature and affect the safety of the crane. Therefore, it is necessary to analyze the influence of temperature on the crane during trolley operation.

Many engineering structures transport moving parts, such as vehicle-bridge systems, projectile-gun systems, weight-bridge crane systems, and slider rail systems, and can be simplified as a moving mass-beam model. In the crane dynamic system, the load state formed by wire rope, hanger, and crane is a major cause of crane vibration, which has been the topic of substantial in-depth research. Huang et al. [17] and Masoud and Nayfeh [18] studied the swing of lifting weights during lifting, simplified the system into a double swing vibration model, and eliminated vibration of the lifting weight by means of feedback control measures. Many studies have also analyzed the dynamic response of the main beam and swing angle of the crane during trolley operation.

A large body of research on the problems of various structures with linear behavior traversed by a moving mass and moving load has been conducted by Frýba [19], specifically for single and multispan beam structures. Regarding the problem of moving loads acting on a Bernoulli–Euler beam, Foda and Young [20] used a dynamic Green function approach to determine the response of a finite length, simply supported Bernoulli–Euler beam subjected to a moving mass traversing its span and analyzed the influences of travelling velocity variations and the ratio of moving mass to beam mass on the dynamic response. They demonstrated the efficiency and simplicity of their method using several numerical examples. Kiani et al. [21, 22] reported a numerical parametric investigation into the design parameters of multispan viscoelastic shear deformable beams subjected to a moving mass via the generalized moving least squares method and another comprehensive parametric investigation on the evaluation of design parameters, where the maximum deflection and bending moment of beams were analyzed. Regarding the problem of moving loads acting on thin beams with geometric nonlinearity, they also employed an efficient meshless method and the reproducing kernel particle method for a spatial discretization nonlinear beam [23].

Although many scholars have studied the influence of moving mass on the dynamic characteristics of the crane main beam, these studies have mainly focused on the situation where the vehicle has a higher moving speed and the moving mass can leave the simply supported beam. The crane structure and trolley operation mode have their own characteristics, yet previous literature does not typically consider the influence of installation location and cabin mode on the dynamic characteristics of the main beam during trolley operation. At the same time, vibrations can lead to occupational injuries for the hoistman. In the existing dynamic analysis of cranes, hoistman vibration is seldom considered, yet the operational comfort of the hoistman directly affects the accuracy and safety of crane operation. In addition, due to the long-term high-temperature working environment of the casting crane, research into the influence of temperature on the mechanical properties of steel has rarely been applied to the dynamic analysis of crane structure. Dynamic studies of crane structure do not consider the influence of temperature on the crane.

Therefore, this study firstly considers the installation location and connection mode of the cabin, as well as other factors, constructs a dynamic model of the main beam system during trolley operation, and discusses the dynamic response and safety of the main beam. The vibration response of the cabin is also obtained. Secondly, the high-temperature modulus of elasticity for Q355 alloy steel is obtained using material mechanical property testing equipment, and the constitutive equation of modulus

elasticity is obtained by data fitting. Test results are validated through a comparison with previous studies. Finally, based on the constitutive equation, the vibration characteristics of the crane beam and cabin at high temperature and the safety of crane are analyzed. This method provides an important theoretical basis for metal structure design, kinematic-dynamic analysis, life prediction, and safety evaluation of casting cranes.

2. Metal Elastic Modulus Analysis

Casting cranes operate in a high-temperature environment lifting molten metal for a long duration. The metal material characteristics of the crane are greatly affected by the temperature field, which will have a substantial impact on the structural performance and operational lifetime of the crane. Therefore, mechanical properties of metal materials are experimentally tested and dynamic responses of the crane system are analyzed at high temperature.

2.1. Trial Objective. Casting cranes are mainly used for lifting ladles containing molten metal. Because of the working location and specific characteristics, there are high requirements for the dynamic characteristics and safety of these cranes. In addition, due to the large size and complex structure of casting cranes, temperature affects the elastic modulus and dynamic structure of the main beam material. This could directly lead to a reduction in the safety factor, which poses a significant threat to the economy and staff safety. Therefore, a test bed is applied to obtain the influence of temperature on the elastic modulus of the steel material and the relationship with time.

2.2. Specimen Design. The specimen material is Q355 low-alloy, high-strength steel. The main chemical composition of this material according to the product quality specifications is shown in Table 1. Because of its elemental content, it is characterized as a qualified product. The processing dimensions of the specimens are strictly in accordance with the requirements of ISO 6892-1 [24] and ISO 783-1 [25]. The thickness, standard distance length, and total length of parallel sections are 3 mm, 100 mm, and 120 mm, respectively. The radius of the transition zone between parallel sections and clamping sections is 18 mm. The clamping length of the pin-shaft connection at both ends of the specimen is 45 mm, and the diameter of the shaft hole is 8 mm. The shape and other dimensions of the specimens are shown in Figure 1. The processing accuracy of the specimens must meet the following requirements:

(1) The absolute error of pin joint processing is less than 0.05 mm

(2) The absolute error of standard distance processing is less than 0.5 mm

(3) The absolute error of thickness processing is less than 0.05 mm

Table 1: Main chemical constituents of the Q355 steel material.

Chemical constituents	C	Mn	Si	S	P
Element content (%)	0.17	1.61	0.43	0.026	0.016

2.3. Test Procedure

2.3.1. Composition of the Test System. The equipment for testing the mechanical properties of the Q355 alloy steel at different temperatures includes three main systems: a structural loading system, a temperature control system, and a data acquisition system. The composition of the test system is shown in Figure 2, and a photograph of the test bench is shown in Figure 3. The main test equipment includes a computer-controlled electronic universal testing machine (UTM6000), electronic extensometer (YSJ50/25-ZC), high-temperature furnace, temperature control device (WGDN-7300L), the material test system, and a DC power supply.

The key equipment performance parameters are as follows:

(1) Computer-controlled electronic universal testing machine (UTM6000): maximum load 1000 kN, with 1% control accuracy of loading

(2) Electronic extensometer (YSJ50/25-ZC): measuring distance 50 mm, maximum range 25 mm, and precision 0.05 mm

(3) Temperature control device (WGDN-7300L): temperature control ranges from 100 to 600°C, temperature deviation < 1.0°C (for temperatures greater than 300°C, the deviation is less than 2.5°C), and temperature fluctuation range < 1.0°C during heat preservation.

2.3.2. Test Method. Firstly, the test equipment is installed and debugged to ensure the safety and accuracy of the test process. Secondly, the specimens are installed on the test machine and maintained in a vertical position. In the temperature measurement system, the coordinates of the high-temperature furnace are adjusted to ensure that the entire specimen is within the high-temperature furnace. The temperature of the specimen is controlled and kept constant for 10 min before the test. Finally, the elastic modulus of the specimens is tested using the loading system, and the test data and images are displayed in the material test software of the electronic universal testing machine.

Casting cranes are mainly used for lifting ladle containing molten metal that will have strong thermal radiation to the crane, which will affect the mechanical properties of the main beam structure. Therefore, in the design of crane, a layer of insulation board made of asbestos mesh is usually applied at the bottom of the main beam, which effectively prevents the partial radiation of temperature field to main beam. Therefore, the maximum temperature of the main beam will not exceed 600°C, and it is even less likely to reach 1000°C. In the test, considering the influence of temperature field on the mechanical properties for main beam structure, the highest test temperature is chosen to be 600°C.

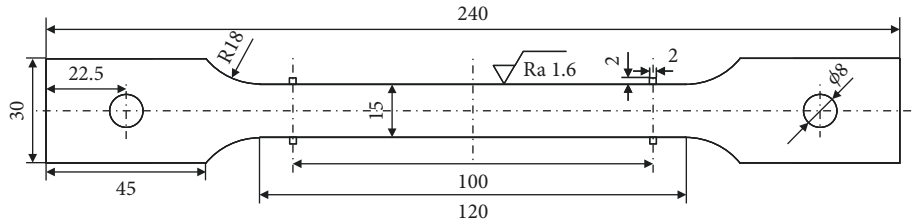

Figure 1: Shape and dimensions of the specimens.

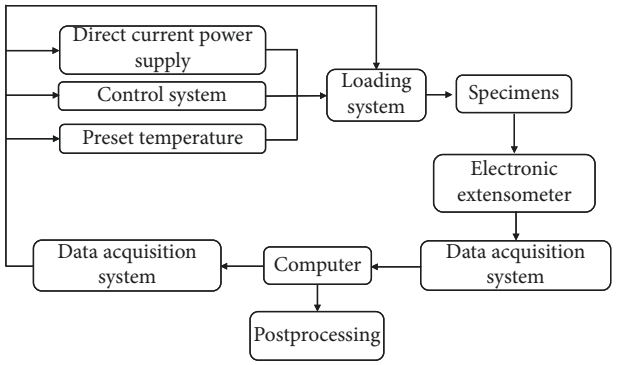

Figure 2: Composition of the test system.

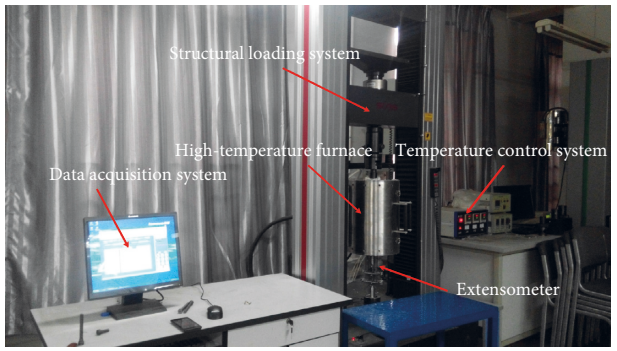

Figure 3: Photograph of the test bed.

2.3.3. Analysis of Test Results. When testing mechanical properties at high temperatures, it is necessary to study the tensile test curve of steel at high temperatures. The stress-strain curves of Q355 alloy steel obtained through tensile tests at different temperatures are shown in Figure 4. It can be seen from the figure that the stress-strain curves of the tensile specimens vary considerably at different temperatures. With the increase in temperature, the yield strength and elastic modulus of Q355 alloy steel show a downward trend. In particular, when $T > 400^{\circ}\text{C}$, the yield strength reduces sharply. At $T = 600^{\circ}\text{C}$, the yield strength is 165 MPa, which is 46.2% of the yield strength (357 MPa) at room temperature.

Deformation of the material prior to yielding is very small, but there is an approximate linear segment. According to the definition of the elasticity modulus at room temperature, the high-temperature stress-strain curve can be obtained as the slope of the approximate straight line when the material is deformed. In general, the ratio of stress to strain is the elastic

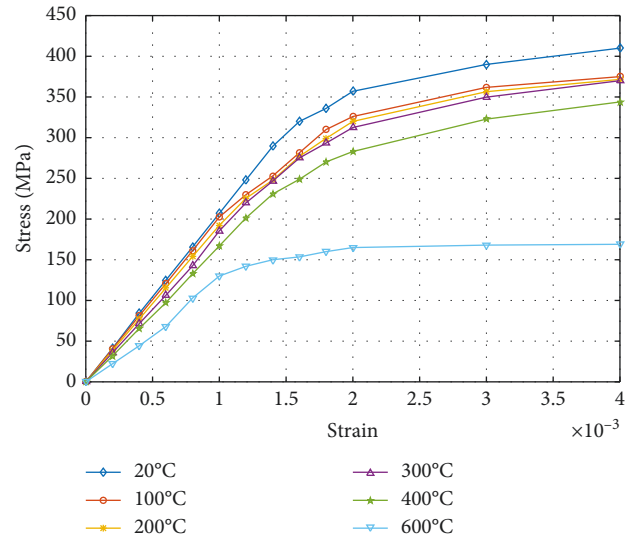

Figure 4: Stress-strain curves of Q355 steel pipe at different temperatures.

modulus in the range of 0.01–0.1%. The measured elastic moduli are listed in Table 2.

Table 2 reveals that the variation of elasticity modulus with temperature is similar to that of strength. With increasing temperatures, the modulus of elasticity decreases gradually. The change of elasticity modulus is reduced in the range of 20–300°C as the temperature increases, and the elasticity modulus decreases at a faster rate at 300–600°C than 20–300°C. At the European Conference on Building Steel Structures, the following expressions were proposed for the relationship between the elastic modulus and temperature of steel structures, as shown in equation (1) [27]; Australian code AS4100 [13] and Trahair [28] suggested that equation (2) is used to calculate the elastic modulus of metal steel structures under different temperature environments:

$$E_T = E\left(1 + 1.59 \times 10^{-4} T - 3.45 \times 10^{-6} T^2 + 1.18 \times 10^{-9} T^3 - 1.72 \times 10^{-11} T^4\right), \quad 0^{\circ}\text{C} < T \le 600^{\circ}\text{C}, \tag{1}$$

$$E_T = E + \frac{ET}{2000}\left[\ln\left(\frac{T}{1100}\right)\right]^{-1}. \tag{2}$$

Table 2: Test values of the modulus of elasticity.

Temperature (°C)	Serial number	Elasticity modulus (×105 MPa)			
		Test values	Average values	Reference [26]	Test error (%)
20	1	2.06	2.06	2.03	1.5
	2	2.06			
	3	2.06			
100	1	2.03	2.03	2.01	1.0
	2	2.02			
	3	2.04			
200	1	1.94	1.93	1.90	1.6
	2	1.92			
	3	1.94			
300	1	1.80	1.79	1.83	2.2
	2	1.79			
	3	1.79			
400	1	1.59	1.59	1.53	3.9
	2	1.58			
	3	1.59			
600	1	1.10	1.11	1.2	7.5
	2	1.10			
	3	1.12			

In [7–9, 26], the elastic modulus and mechanical properties of steel structures at different temperatures were measured experimentally. The equations for elastic modulus calculation at different temperatures, obtained by fitting these discrete data, are shown below (equations (3)–(6)):

$$E_T = \begin{cases} E - 4.86 \times 10^{-4} T, & 0 < T \le 370^{\circ}\mathrm{C}, \\ (1.515 - 1.879 \times 10^{-3} T) E, & 370^{\circ}C < T \le 700^{\circ}\mathrm{C}, \end{cases} \tag{3}$$

$$E_T = \frac{E}{1.03 + 7 \times 10^{-17} (T - 20)^6}, \quad 20^{\circ}\mathrm{C} < T \le 600^{\circ}\mathrm{C}, \tag{4}$$

$$\begin{aligned} E_T = E \Big[& 0.911 - 5.896 \times 10^{-4} (T - 308.57) - 2.2 \times 10^{-6} (T - 308.57)^2 \\ & - 9.652 \times 10^{-9} (T - 308.57)^3 - 1.88 \times 10^{-11} (T - 308.57)^4 \Big], \quad T \le 600^{\circ}\mathrm{C}, \end{aligned} \tag{5}$$

$$\begin{aligned} E_T = E \Big(& 1.0829 - 0.0016T + 8.7 \times 10^{-6} T^2 \\ & - 2.53 \times 10^{-8} T^3 + 2.155 \times 10^{-11} T^4 \Big), \quad 100^{\circ}\mathrm{C} \le T \end{aligned} \tag{6}$$

As mentioned in the Technical Specification for Fire Protection of Building Steel Structures (GB 51249-2017), the elastic modulus of ordinary steel at high temperature can be calculated according to the following equation [16]:

$$E_T = \begin{cases} \dfrac{7T - 4780}{6T - 4760} E, & 20^{\circ}\mathrm{C} < T \le 600^{\circ}\mathrm{C}, \\ \dfrac{1000 - T}{6T - 2800} E, & 600^{\circ}\mathrm{C} < T \le 1000^{\circ}\mathrm{C}. \end{cases} \tag{7}$$

In Eurocode 3 [12], steel elastic modulus at different temperatures is given. Based on four polynomial fitting methods, the elastic modulus of ordinary steel at high temperature can be calculated according to the following equation:

$$\begin{aligned} E_T = {} & 1.9824 \times 10^{11} + 2.2024 \times 10^{8} T - 1.4746 \times 10^{6} T^2 \\ & + 1542.4 T^3 - 0.48271 T^4. \end{aligned} \tag{8}$$

The elastic modulus of Q355 steel cannot be tested at each corresponding temperature due to the limitations of the experimental conditions. Therefore, based on the elastic modulus obtained from the tensile test at the corresponding temperature, the constitutive equations for the elastic modulus of Q355

steel at different temperatures are fitted by the polynomial fitting method. The fitted constitutive equation is as follows:

$$E_T = 2.063 \times 10^{11} - 7.068 \times 10^6 T - 2.829 \times 10^5 T^2 - 57.33T^3 + 0.1785T^4. \quad (9)$$

By comparing the predicted values of the constitutive equation with the experimental data, it is found that the maximum error is 0.21%, and the predicted results are satisfactory. By comparing the experimental data from the literature with the fitting equation of this study, the relationship between the elastic modulus of metals and temperature is obtained (Figure 5). The fitting curve of the constitutive equation for the elastic modulus of Q355 steel very closely coincides with the experimental value, which reveals the complex nonlinear relationship between temperature and elastic modulus in Q355 steel. At the same time, the experimental and predicted results in this study are consistent with those in other literature. Within a certain temperature range, the trend of the curve is that the elastic modulus of steel decreases with the temperature increase.

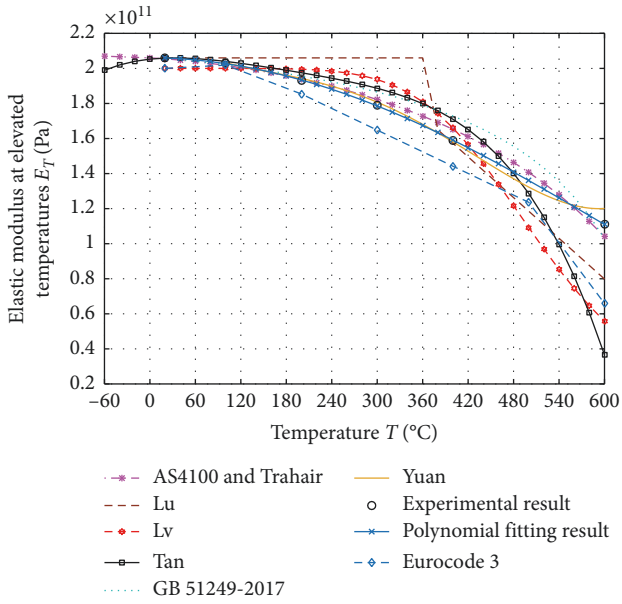

Figure 5: Relationships between the elastic modulus of steel and temperature for selected designs.

3. Crane Dynamic Model considering Cabin Factors

Typically, the installation position of the cabin is located on the side of the main beam of the crane, which is equivalent to hanging a centralized mass on the main beam. With the continuous advancement of intelligent processes, the installation position and installation mode of the cabin are constantly changing. The design of the cabin is related to the physical health, mental health, and operation accuracy of the hoistman. Existing crane models do not take into account the mass m_p and swing angle θ_x of the payload; thus, without considering factors such as cab weight, connection mode, and installation position, the existing mathematical model cannot replicate the actual working conditions of the crane. Therefore, a physical model that more closely simulates the actual working conditions of the crane (Figure 6) is proposed [29].

According to the crane system dynamics model during the operation of trolley shown in Figure 6, the forces on the system mainly include the gravity loads, inertial force, structural elastic force, and dissipative force of each component. The gravity of the system is composed of the gravity of trolley, payload, main beam, and cabin. The inertial force of the system is made up of the inertial force along the Z-axis of trolley, the cabin, main beam, and the inertial force of payload along the Z-axis and swinging inertial force around the Y-axis. The structural elastic force of the system includes the elastic force of the main beam along the Z-axis and the elastic force between cabin and main beam. The dissipative force of the system is consisted of dissipative forces of main beam structure and connection structure between cabin and main beam.

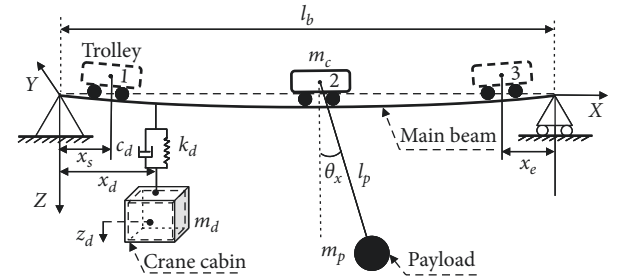

Figure 6: Physical model of crane vibration due to a moving trolley.

3.1. Description of the System Model. A casting crane consists of a frame structure, trolley running mechanism, cab, and lifting weight. According to the size and structural characteristics of components and to simplify the calculation process, the dynamic vibration model of the casting crane system is based on the following assumptions:

(1) As a flexible body, the main beam only considers vertical vibration, assuming that all dampers in the elastic body are viscous dampers, and the dampers in the beam have little influence on structural vibration [30]. Typically, the damping ratio is 0.1–0.7%。.

(2) The cabin is simplified as a lumped mass, only considering vertical vibration, and the connection between cabin and main beam is simplified as a spring and damping system with greater stiffness.

(3) The suspension rope is assumed to be a mass-free rigid suspension rope according to the actual operational characteristics of the bridge crane load operation.

(4) The lifting weight is simplified as a swinging concentrated mass, which is suspended on the mass block by a rigid suspension rope without mass. It moves together with the mass block and swings in the plane.

(5) In the dynamic response analysis of the casting crane, the deflection of the main beam is assumed to be linear, while the influence of nonlinear deflection

of the main beam on the dynamic characteristics of the main beam and cabin is neglected.

Based on the properties of the Euler–Bernoulli beam, the model of trolley travel on the crane beam can be simplified to that of a moving mass on a simply supported beam. That is to say, the bending stiffness is calculated without considering the shear stiffness and torsional stiffness of the beam. The definitions of the parameter symbols used in Figure 6 are given in Table 3.

3.2. Motion Equations of Crane System. The continuous mass of crane structure is distributed along the axial direction of structure and belongs to the system of infinite degrees of freedom. Its dynamic characteristics and responses are generally difficult to be solved. In engineering, the continuous system of distributed quality is often discretized and transformed into a multi-degree-of-freedom discrete system for analysis to obtain a realistic approximate solution. Modal superposition is a fast solution to solve the linear dynamic problem and conduct the transient analysis of the effective solution method. It is obtained by multiplying each mode shape by modal analysis and multiplying the coefficients to calculate the dynamic response.

Many literatures use the modal assumption method to give the vibration displacement of the main beam under the action of moving mass. The calculation accuracy of the modal superposition method in dynamic response analysis of the main beam can meet the engineering calculation accuracy requirements [31]. The vibration of the main beam can be considered as the sum of multiple modal vibrations. The system is simplified to the $N+2$-degree-of-freedom system, rather than a continuous system. As a part of the system, the crane girder structure is simplified into a simply supported homogeneous continuous subsystem. This subsystem is used as the research object to study the response of the main beam structure system at different temperatures under the impact of trolley operation. When the modal order N of the crane main beam approaches positive infinity, the response result is infinitely approximated to the exact solution. When N is a certain value, the response result of the crane main beam is an approximate solution. Based on the regular mode function of the simply supported beam and principle of main beam vibration under moving mass in literatures [32, 33], when the trolley runs at maximum speed, V_m, on the main beam, the elastic displacement curve of the position x in the Z direction of the main beam at time t can be expressed as follows [34, 35]:

$$w(x,t) = \sum_{i=1}^{N} \phi_i(x) q_i(t), \tag{10}$$

where $\phi_i(x) = \sin(i\pi x/l_b)$ is the ith modal of the simply supported beam and $q_i(t)$ and N are the generalized coordinates and coordinate numbers of the elastic displacement of the main beam, respectively. The coordinate vectors can be defined according to the simplified physical model shown in Figure 1. Therefore, the position vector of an elemental mass of the beam, $\bar{r}_b$, the position vector of the carriage, $\bar{r}_c$, the position vector of the payload, $\bar{r}_p$, and the position vector of the crane cabin, $\bar{r}_d$, can be expressed as follows:

Table 3: Notation and meanings of parameters.

Notation	Meaning
E_T	Young's modulus for temperature T
ρ	Volume density
A	Cross-sectional area
l_b	Beam span
x_d	Mounting position of cabin
l_p	Length of wire rope
c_d	Connection damping between cabin and beam
x_e	Extreme right position of trolley
ξ_i	ith damping ratio of beam
i	Unit vectors defined along the X-axis
I_y	Second moment of area
m_c	Mass of the trolley
m_p	Mass of the payload
m_b	Mass of unit length for beam
V_m	Maximum running speed of trolley
θ_x	Swinging angle of the payload
k_d	Connection stiffness between cabin and beam
m_d	Mass of cabin
x_s	Extreme left position of trolley
k	Unit vectors defined along the Z-axis

$$\begin{aligned}
\bar{r}_b &= x \cdot i + w(x,t) \cdot k,\\
\bar{r}_c &= x_c \cdot i + w(x_c,t) \cdot k,\\
\bar{r}_p &= \left(x_c + l_p \sin\theta_x\right) \cdot i + \left(w(x_c,t) + l_p \cos\theta_x\right) \cdot k,\\
\bar{r}_d &= x_d \cdot i + \left(z_d - w(x_d,t)\right) \cdot k.
\end{aligned} \tag{11}$$

Assuming that the total kinetic energy of the system is T, the energy of the two main beams is T_b, the kinetic energy of the running trolley is T_c, and the kinetic energy of the lifting weight is T_p; thus, the kinetic energy of each part of the system can be expressed as follows:

$$\begin{aligned}
T_b &= \frac{1}{4} m_b l_b \sum_{i=1}^{N} \dot{q}_i^2,\\
T_c &= \frac{1}{2} m_c \left\{ \dot{x}_c^2 + \left[\dot{x}_c \sum_{i=1}^{N} \phi_i'(x_c) q_i(t) + \sum_{i=1}^{N} \phi_i(x_c) \dot{q}_i \right]^2 \right\},\\
T_p &= \frac{1}{2} m_p \left\{ \left[\dot{x}_c \sum_{i=1}^{N} \phi_i'(x_c) q_i(t) + \sum_{i=1}^{N} \phi_i(x_c) \dot{q}_i \right]^2 + \dot{x}_c^2 \right.\\
&\quad + l_p^2 \dot{\theta}_x^2 + 2 l_p \dot{x}_c \dot{\theta}_x \cos\theta_x - 2 l_p \dot{\theta}_x \sin\theta_x\\
&\quad \left. \cdot \left[\dot{x}_c \sum_{i=1}^{N} \phi_i'(x_c) q_i(t) + \sum_{i=1}^{N} \phi_i(x_c) \dot{q}_i \right] \right\},\\
T_d &= \frac{1}{2} m_d \left\{ \left[\sum_{i=1}^{N} \phi_i(x_d) \dot{q}_i(t) \right]^2 - 2 \dot{z}_d \sum_{i=1}^{N} \phi_i(x_d) \dot{q}_i(t) + \dot{z}_d^2 \right\}.
\end{aligned} \tag{12}$$

In the coupled system model, the system potential energy includes the elastic strain energy of the main beam, the elastic potential energy of the spring between the main beam

and cabin, and the work done by the gravity of the trolley, cabin, and lifting weight itself. Therefore, the potential energy in the system, U, can be expressed as follows:

$$U = \frac{E_T I_y \pi^4}{4l_b^3} \cdot \sum_{i=1}^{N} i^4 q_i^2(t) - \left(m_c + m_p\right) g \cdot \sum_{i=1}^{N} \phi_i(x_c) q_i(t) - m_p g l_p \cos\theta_x - m_d g z_d + \frac{1}{2} k_d \left[z_d - \sum_{i=1}^{N} \phi_i(x_d) q_i(t) \right]^2. \tag{13}$$

The dissipated energy in the system, D, can be expressed as follows:

$$D = \frac{1}{2} \sum_{i=1}^{N} c_i \dot{q}_i^2(t) + \frac{1}{2} c_d \left(\dot{z}_d - \sum_{i=1}^{N} \phi_i(x_d) \dot{q}_i(t) \right)^2. \tag{14}$$

The Lagrange equation of nonconservative systems can be expressed as follows:

$$\frac{\mathrm{d}}{\mathrm{d}t}\left(\frac{\partial T}{\partial \dot{y}_i}\right) - \frac{\partial T}{\partial y_i} + \frac{\partial U}{\partial y_i} + \frac{\partial D}{\partial \dot{y}_i} = F_i, \quad (i = 1, 2, \ldots, n), \tag{15}$$

where $\partial D/\partial \dot{y}_i$ is the damping force caused by the energy dissipation function D, F_i only represents the generalized excitation force of external action, y_i is the generalized coordinate, and $\dot{y}_i$ is the generalized velocity.

According to equation (15) and the modal assumption principle, the main beam is simplified to the j-order modal superposition form. Therefore, the number of vibration equations for the main beam is j, and the vibration differential equation can be unified into the following form:

$$\begin{aligned}
&\frac{1}{2} m_b l_b \ddot{q}_j + \left(m_c + m_p\right) \cdot \phi_j(x_c) \sum_{i=1}^{N} \phi_i(x_c) \ddot{q}_i + m_d \phi_j(x_d) \sum_{i=1}^{N} \phi_i(x_d) \ddot{q}_i \\
&+ 2\left(m_c + m_p\right) \cdot \phi_j(x_c) \dot{x}_c \sum_{i=1}^{N} \phi_i'(x_c) \dot{q}_i + 2\xi_j m_b l_b \omega_j \dot{q}_j + c_d \phi_i(x_d) \sum_{i=1}^{N} \phi_i(x_d) \dot{q}_i(t) \\
&+ \left(m_c + m_p\right) \cdot \phi_j(x_c) \left(\ddot{x}_c \sum_{i=1}^{N} \phi_i'(x_c) q_i(t) + \dot{x}_c^2 \sum_{i=1}^{N} \phi_i''(x_c) q_i(t) \right) \\
&+ k_d \phi_j(x_d) \sum_{i=1}^{N} \phi_i(x_d) q_i(t) + \frac{E I_y \pi^4 j^4}{2 l_b^3} q_j - \left(m_c + m_p\right) g \phi_j(x_c) \\
&- k_d z_d \phi_j(x_d) - m_p \cdot l_p \phi_j(x_c) \left(\ddot{\theta}_x \sin\theta_x + \dot{\theta}_x^2 \cos\theta_x \right) - m_d \phi_j(x_d) \ddot{z}_d - c_d \phi_j(x_d) \dot{z}_d = 0.
\end{aligned} \tag{16}$$

According to equation (16), the differential equation of vibration for the main beam can be deduced as follows:

$$\mathbf{M}\ddot{\mathbf{q}}(t) + \mathbf{C}\dot{\mathbf{q}}(t) + \mathbf{K}\mathbf{q}(t) = \mathbf{F}(t), \tag{17}$$

where $\mathbf{M}$, $\mathbf{C}$, and $\mathbf{K}$ are the mass matrix, damping matrix, and stiffness matrix, respectively; $\ddot{\mathbf{q}}(t)$, $\dot{\mathbf{q}}(t)$, and $\mathbf{q}(t)$ are the acceleration vector, velocity vector, and displacement vector of the system, respectively; and $\mathbf{F}(t)$ is a load vector. The mass matrix, damping matrix, stiffness matrix, and excitation force vector in the system vibration equation can be expressed as follows:

$$\mathbf{M} = \begin{bmatrix}
1 + P_M\varphi_{11c} + D_M\varphi_{11d} & P_M\varphi_{12c} + D_M\varphi_{12d} & \cdots & P_M\varphi_{1Nc} + D_M\varphi_{1Nd} \\
P_M\varphi_{21c} + D_M\varphi_{21d} & 1 + P_M\varphi_{22c} + D_M\varphi_{22d} & \cdots & P_M\varphi_{2Nc} + D_M\varphi_{2Nd} \\
\vdots & \vdots & \ddots & \vdots \\
P_M\varphi_{NNc} + D_M\varphi_{NNd} & P_M\varphi_{N2c} + D_M\varphi_{N2d} & \cdots & 1 + P_M\varphi_{NNc} + D_M\varphi_{NNd}
\end{bmatrix}, \tag{18}$$

$$\mathbf{C} = \begin{bmatrix}
C_{11} + 4\xi_1\omega_1 & C_{12} & \cdots & C_{1N} \\
C_{21} & C_{22} + 4\xi_2\omega_2 & \cdots & C_{2N} \\
\vdots & \vdots & \ddots & \vdots \\
C_{N1} & C_{N2} & \cdots & C_{NN} + 4\xi_N\omega_N
\end{bmatrix}, \tag{19}$$

$$\mathbf{K} = \begin{bmatrix} K_{11} + \dfrac{E_T I_y \pi^4}{m_b l_b^4} & K_{12} & \cdots & K_{1N} \\ K_{21} & K_{22} + \dfrac{E_T I_y \pi^4 2^4}{m_b l_b^4} & \cdots & K_{2N} \\ \vdots & \vdots & \ddots & \vdots \\ K_{N1} & K_{N2} & \cdots & K_{NN} + \dfrac{E_T - I_y \pi^4 N^4}{m_b l_b^4} \end{bmatrix}, \tag{20}$$

$$\mathbf{F}(t) = \begin{pmatrix} \phi_1(x_c)\left(P_M g + R_M\left(\ddot{\theta}_x \sin\theta_x + \dot{\theta}_x^2 \cos\theta_x\right)\right) + \phi_1(x_d)\left(D_M \ddot{z}_d + K_d z_d + C_d \dot{z}_d\right) \\ \phi_2(x_c)\left(P_M g + R_M\left(\ddot{\theta}_x \sin\theta_x + \dot{\theta}_x^2 \cos\theta_x\right)\right) + \phi_2(x_d)\left(D_M \ddot{z}_d + K_d z_d + C_d \dot{z}_d\right) \\ \vdots \\ \phi_N(x_c)\left(P_M g + R_M\left(\ddot{\theta}_x \sin\theta_x + \dot{\theta}_x^2 \cos\theta_x\right)\right) + \phi_N(x_d)\left(D_M \ddot{z}_d + K_d z_d + C_d \dot{z}_d\right) \end{pmatrix}, \tag{21}$$

where $C_{ij} = 2P_M \dot{x}_c \varphi_{ijc1} + C_d \varphi_{ijd}\,(i, j = 1, 2, \ldots, N)$,

$$K_{ij} = P_M \ddot{x}_c \varphi_{ijc1} + P_M \dot{x}_c^2 \varphi_{ijc2} + K_d \varphi_{ijd}, \quad (i, j = 1, 2, \ldots, N),$$

$$P_M = \frac{2\left(m_c + m_p\right)}{m_b l_b},$$

$$D_M = \frac{2m_d}{m_b l_b},$$

$$R_M = \frac{2m_p \cdot l_p}{m_b l_b},$$

$$\varphi_{mnc1} = \phi_m(x_c)\phi_n'(x_c),$$

$$\varphi_{mnc2} = \phi_m(x_c)\phi_v''(x_c),$$

$$K_d = \frac{2k_d}{m_b l_b},$$

$$C_d = \frac{2c_d}{m_b l_b},$$

$$\varphi_{mnc} = \phi_m(x_c)\phi_n(x_c),$$

$$\varphi_{mnd} = \phi_m(x_d)\phi_n(x_d). \tag{22}$$

According to equation (15), the differential equation of payload swing can be deduced as follows:

$$l_p \ddot{\theta}_x - \left[\left(\dot{x}_c \sum_{i=1}^{N} \phi_i'(x_c)\dot{q}_i + \sum_{i=1}^{N} \phi_i(x_c)\ddot{q}_i\right) + \ddot{x}_c \sum_{i=1}^{N} \phi_i'(x_c) q_i(t) + \dot{x}_c\left(\dot{x}_c \sum_{i=1}^{N} \phi_i''(x_c) q_i(t) + \sum_{i=1}^{N} \phi_i'(x_c)\dot{q}_i(t)\right)\right]\sin\theta_x + g\sin\theta_x + \ddot{x}_c \cos\theta_x = 0, \tag{23}$$

and the differential equation of cabin vibration is given as follows:

$$m_d\left[\ddot{z}_d - \sum_{i=1}^{N} \phi_i(x_d)\dot{q}_i(t)\right] + k_d z_d - k_d \sum_{i=1}^{N} \phi_i(x_d) q_i(t) - m_d g + c_d \dot{z}_d - c_d \sum_{i=1}^{N} \phi_i(x_d)\ddot{q}_i(t) = 0. \tag{24}$$

3.3. Procedure and Reliability Analysis of the Solution. Nonlinear factors exist widely in engineering and include the nonlinearity of materials such as nonlinear forces, motion nonlinearity, nonlinear constitutive relationships, and geometric nonlinearity such as large elastic deformation. From a mathematical point of view, equation (17) is a second-order ordinary differential equation, which can be solved by the Runge–Kutta method. However, when the order of the matrix in the motion equation is large, the efficiency of this method is very low. The mode superposition method and direct integration method can effectively overcome the shortcomings of a slow solution process and improve calculation efficiency. These two methods are widely used in engineering to solve the numerical solution of dynamic problems. Formula (16) constitutes a two-dimensional system of second-order nonlinear time-varying differential equations. The direct integration method is effective for second-order nonlinear vibration systems, which has been verified in many studies [36, 37]. In this study, the Newmark direct integration method is used to approximate the vibration response of the system. Under the action of a moving trolley, the flow chart of the dynamic response of the main beam and cabin is shown in Figure 7, and the calculation process is as follows:

(1) Firstly, the system motion equation is established according to the system model and Lagrange equation, and the initial values of the vibration responses for the main beam are set to $\ddot{\mathbf{q}}_0$, $\dot{\mathbf{q}}_0$, and $\mathbf{q}_0$,

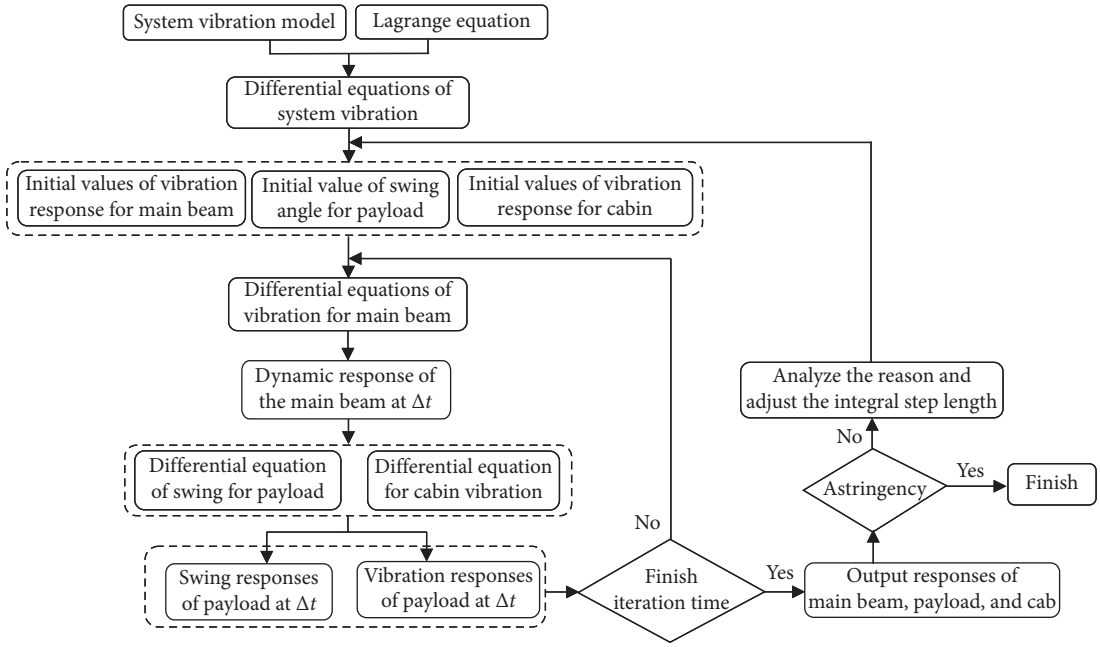

Figure 7: Calculation processes of nonlinear vibration equations.

the initial values of the swing angle of the payload $\ddot{\theta}_{x0}$, $\dot{\theta}_{x0}$, and θ_{x0} are set to zero, and the initial values of cabin vibration response $\ddot{z}_{d0}$, $\dot{z}_{d0}$, and z_{d0} are all zero. The dynamic responses $\ddot{\mathbf{q}}_{\Delta t}$, $\dot{\mathbf{q}}_{\Delta t}$, and $\mathbf{q}_{\Delta t}$ at Δt time in equation (17) are calculated based on the Newmark method.

(2) The results obtained in the first step are substituted into equations (23) and (24), and the payload angle responses $\ddot{\theta}_{x\Delta t}$, $\dot{\theta}_{x\Delta t}$, and $\theta_{x\Delta t}$ of the crane are calculated by the Newmark method. The cabin vibration responses are also obtained.

(3) The results obtained in Step (2) are substituted as the initial value of the next iteration into Step (1) to calculate the vibration response of the main beam at the next moment, and Step (2) is repeated. Calculation Steps (1) and (2) are iterated until the preset termination time, and the numerical solutions of the beam, swing angle of the crane, and cabin vibration are obtained.

(4) The convergence of calculation results $\ddot{\mathbf{q}}(t)$, $\ddot{\theta}_x(t)$, and $\ddot{z}_d(t)$ is tested. If they do not converge, return to Step (2) for further analysis and calculation.

3.4. Verification of Model Validity

3.4.1. Verification of Main Girder Vibration Response. To further confirm the reliability of the presented formulae and the developed computer programs, a pinned-pinned beam subjected to a moving mass $m = 70\,\text{kg}$ and constant speed of $V_{mx} = 3.34\,\text{m/s}$ was also investigated. The length of the beam was $L_b = 10\,\text{m}$, the cross-sectional area was $A = 9.0024 \times 10^{-4}\,\text{m}^2$, and second moment of area was $I = 1.04 \times 10^{-6}\,\text{m}^4$. The mass density was $\rho = 7820\,\text{kg/m}^3$, and Young's modulus was $E = 2.068 \times 10^{11}\,\text{N/m}^2$. The above information of the beam was almost the same as references [38, 39].

Figure 2 shows the time histories for the vertical central displacements of the pinned-pinned beam. In reference [39], the influence of the moving mass on the midpoint shape of the simply supported beam was solved by using finite element theory. Additionally, in reference [38], the dynamic response of the middle point of the main beam was solved under a modal assumption. However, in this study, the time-domain response of the midpoint vibration of the main beam was solved by combining the modal hypothesis with the energy conservation of the system. As can be seen from Figure 8, three calculation results were consistent with the underlying trend. Since the differences between the last three curves were small, the formulations and computer programs developed in this study should be available for calculating the dynamic responses of a structure due to a moving load.

3.4.2. Verification of Swing Angle. The payload swing is affected by the carriage traverse acceleration and the length of the wire rope. The reliability of the presented formulae and the developed computer programs were further confirmed with regard to the swing angle. A pinned-pinned beam was subjected to a moving mass of $m_c = 97.9\,\text{kg}$ and a payload mass of $m_p = 97.9\text{kg}$. The beam had a length of $l_b = 6\,\text{m}$, cross-sectional area of $A = 2.04 \times 10^{-2}\,\text{m}^2$, and second moment of area $I = 2.13 \times 10^{-7}\,\text{m}^4$. The mass density was $\rho = 8000\,\text{kg/m}^3$, and Young's modulus was $E = 2.11 \times 10^{11}\,\text{N/m}^2$. In practice, the carriage starts with an initial velocity of zero and accelerates to a particular speed, which could be held constant for some time before decelerating to rest. In all cases, the terminal times of the intervals were $t_1 = 15\,\text{s}$, $t_2 = 45\,\text{s}$, and $t_3 = 60\,\text{s}$, the speed during the constant speed phase was $V = 0.1333\,\text{m/s}$, and the

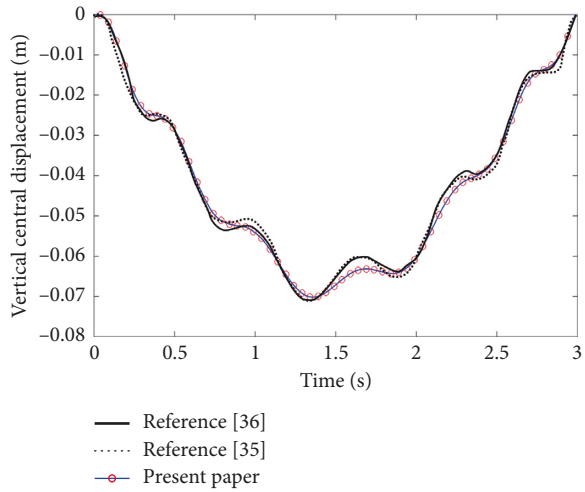

Figure 8: Calculation results of central displacement position deflection compared to references [38, 39].

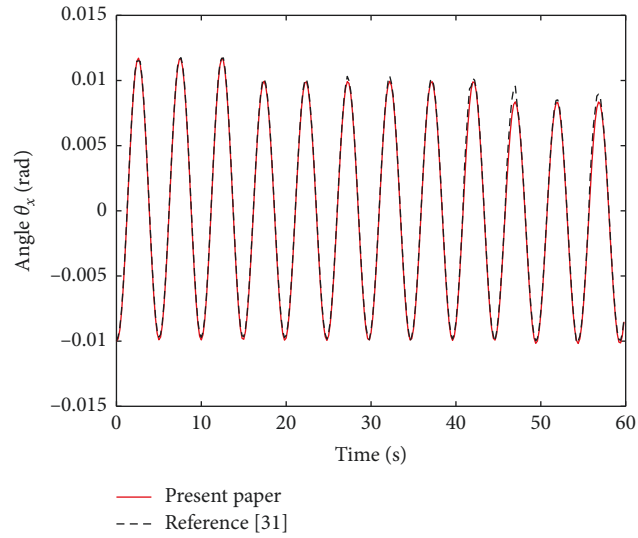

Figure 9: Consistency comparison of calculated results to Reference [31].

deceleration phase occurred over the last meter of the motion. The initial displacements for each swing angle were $\theta_x(0) = -0.01$ (rad).

The mass of the cabin, connection stiffness, and damping, were all set to zero. By ignoring the structural damping effect, the factors were considered to be consistent with those reported in [31]. From Figure 9, it can be seen that the results of this study are similar to those reported in [31], which proves the validity of the calculation principle and procedure.

4. Engineering Applications

A 100/40t – 28.5 m casting crane as an example is selected. During service, rail defects are caused by foundation subsidence, which leads to strong hoistman vibration and equipment damage. The initial parameters of the crane vibration system are listed in Table 4.

Table 4: Parameter values of the rigid flexible coupling system of the casting crane [29].

Parameters	Values
m_c	20000 kg
m_p	20000 kg
ρ	7820 kg/m^3
E	2.06 × 1011 N/m^2
I	0.0093 m^4
x_s	2.25 m
l_b	28.5 m
l_p	5.7 m
ξ_i	0.001
g	9.81 N/kg
A	0.128 m^2
x_e	2.25 m
k_d	108 N/m
c_d	105 N s/m
x_d	5 m
m_d	2000 kg
$V_{\max}$	72 m/min
θ_x	0 rad

4.1. Trolley Operation Modes. Compared with other cranes, the ladle lifted by the casting crane is a very dangerous piece of equipment. The excessive speed of operation can produce an excessive swing angle of the ladle, which greatly reduces the safety of the production process. The relevant operating parameters of the trolley can be found in the standard [40, 41], and the maximum speed of the trolley is 63 m/min. However, the running speed may be larger than this value in special cases. The maximum speed of the trolley is less than that of other cranes at approximately 80 m/min. According to the operation speed of the casting crane provided by a certain company and combined with the most dangerous working conditions, three running speed modes of the trolley system are shown in Figure 10 based on literature [39, 42]. Three modes of operation that have a higher frequency of occurrence in actual crane operation are derived from a company.

The acceleration and deceleration time of the trolley is set to 5 s, and the trajectory of the trolley extends from the limit position on one side to the limit position on the other side. The maximum running speed of the trolley is set to $V_{\mathrm{m}}^3 = 1.2$ m/s. If the trolley runs safely in this mode, the stability of the other two modes can be guaranteed, thus ensuring trolley safety during operation. The results in the following sections are based on these three modes of trolley operation.

4.2. Main Beam Dynamic Response to Temperature. Because temperature has a large influence on the elastic modulus and mechanical properties of metal structures, and the casting crane operates under high temperature, it is necessary to analyze the dynamic characteristics of the main girder under the action of temperature. According to the literature [26], the elastic modulus of the main beam decreases substantially at temperatures above

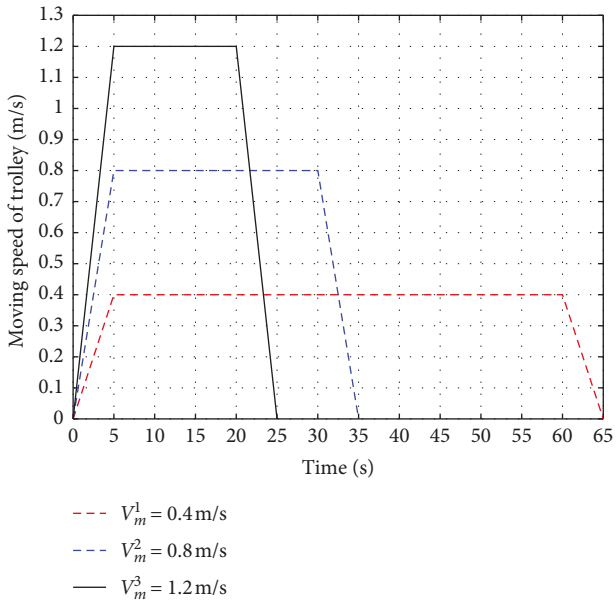

Figure 10: Three speed patterns of the moving trolley.

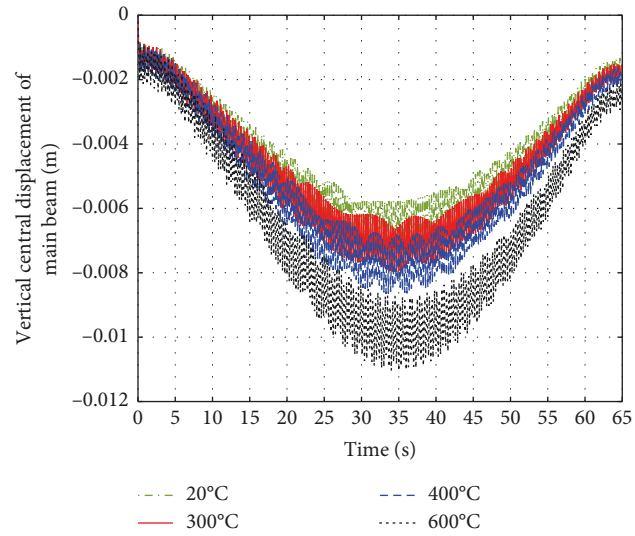

Figure 11: Displacement response of the main beam at different temperatures.

300°C, so the midspan displacement of the main beam is significantly increased. Therefore, the temperature of the main beam in the midspan response calculation should be above 300°C. The parameters of the crane are selected, and the dynamic response of the main girder in the midspan is calculated according to the elastic modulus at different temperatures obtained from the test (Figure 11). The maximum displacement of the main girder beam is 7 mm and 11 mm at 20°C and 600°C, respectively. The vertical center displacement of the main beam increases by 57.1% at 600°C than 20°C. More importantly, when the crane runs at full load, the increase of midspan displacement may directly lead to deformation of the crane beam that exceeds the maximum allowable displacement of the crane; this poses a major threat to humans and property. Therefore, the influence of temperature on the dynamic characteristics of the main beam must be considered during the design stage of the crane.

Under the initial parameters of Table 4, equation (9) is employed to calculate the elastic modulus at different temperatures, and the dynamic characteristics of the main beam are obtained by varying the temperature, as shown in Figure 12. With increasing temperature, the maximum midspan displacement of the main beam increases gradually. This is because high temperature tends to decrease the elastic modulus of the main beam, resulting in a reduction of main beam stiffness, which causes an increase of the midspan displacement amplitude of the main beam during trolley operation.

4.3. Cabin Dynamic Response to Temperature

4.3.1. Cabin Displacement Response. The cabin vibration response at different temperatures is shown in Figure 13. The maximum amplitude of cabin vibration is 3 mm and 4.3 mm at 20°C and 600°C, respectively. The vibration displacement of the cabin increases by 32.5% with increasing temperature. The amplitude of cabin vibration will have a clear impact on human vibration comfort.

4.3.2. Cabin Acceleration Response. The acceleration response results are shown in Figure 14, indicating that the maximum acceleration of the cabin is 2.45 m/s^2, 2.25 m/s^2, 2.25 m/s^2, and 2.5 m/s^2 at 20°C, 300°C, 400°C, and 600°C, respectively. Although temperature has a significant influence on vibrational displacement of the main beam and cabin, the influence of temperature on vibrational acceleration of the cabin, which directly affects the comfort of the hoistman, is not significant.

4.4. Influence of Yield Strength on Crane Structure Safety. The yield strength will have a certain influence on the safety of crane metal structures. According to the design method of metal structure for the mechanical equipment, the calculated stress of the dangerous position for the casting crane can be calculated according to the following equation:

$$\sigma = \frac{N}{A_j} + \frac{M}{w_j} \leq [\sigma], \tag{25}$$

where σ is the calculated stress of the structure, N is the axial force of the structure, A_j is the net area of the structural calculation section, M is the basic bending moment of the calculated section, w_j is the net bending section coefficient of the calculated section, and $[\sigma]$ is the allowable stress.

When the ratio of yield strength to ultimate strength is greater than or equal to 0.7, the allowable stress of crane metal structure can be obtained according to the following equation:

$$[\sigma] = \frac{0.5\sigma_s + 0.35\sigma_b}{n_i}, \tag{26}$$

where σ_s is the yield strength of steel, σ_b is the ultimate strength of steel, and n_i is the safety factor. Since the casting

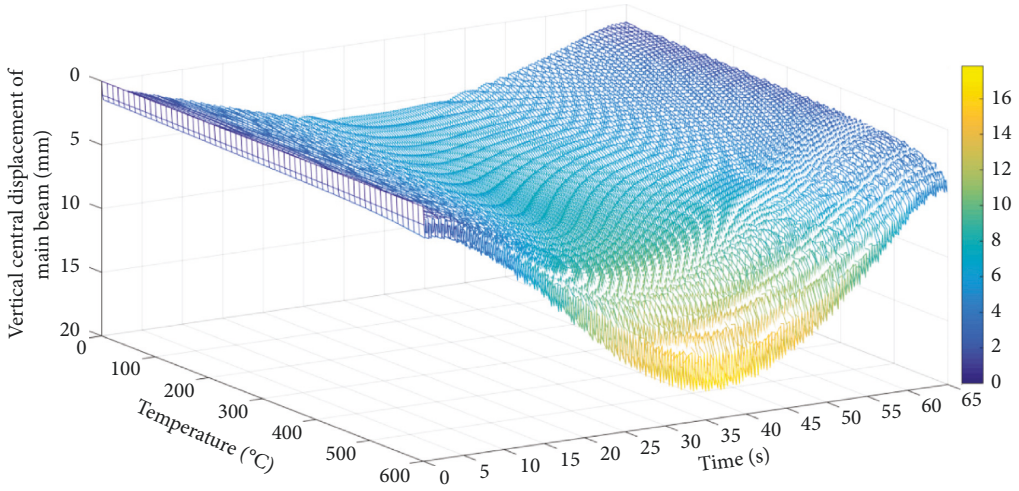

Figure 12: 3-D graph of the domain response of the main beam at different temperatures.

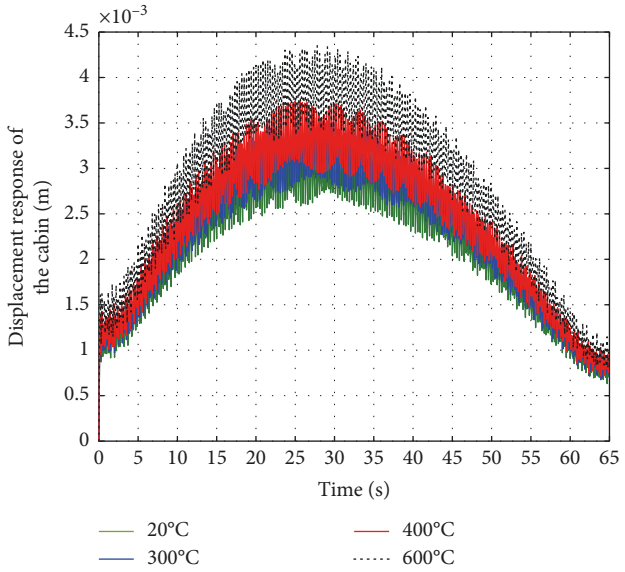

Figure 13: Displacement response of the cabin at different temperatures.

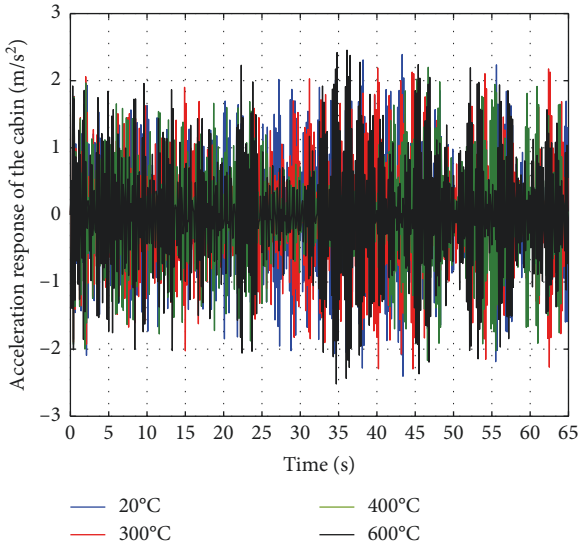

Figure 14: Acceleration response of the cabin at different temperatures.

Table 5: Structural stress and safety evaluation results of main beam at different temperatures.

Temperature (°C)	Elastic modulus (MPa)	Yield strength (MPa)	Tensile strength (MPa)	Allowable stress (MPa)	Calculated stress (MPa)	Safety margin (MPa)	Evaluation result
20	$2.06E+05$	357	410	217.56	124.3	93.26	Safety
100	$2.03E+05$	326	375	198.81		74.51	Safety
200	$1.93E+05$	320	371.6	195.98		71.68	Safety
300	$1.79E+05$	312.5	370	193.07		68.77	Safety
400	$1.59E+05$	283	343.9	176.93		52.63	Safety
600	$1.11E+05$	165	169	95.70		−28.6	Failure

crane is in a room without wind, based on load combination A, the value of n_i is 1.48 [43].

Equation (26) is used to calculate the allowable stress of the cast crane metal structure at different temperatures. Based on test results in Section 2.3.3 of the manuscript, the structural stress and safety evaluation results of the main beam at different temperatures are shown in Table 5.

As presented in Table 5, the safety margin of crane structure decreases with increasing temperature. When the temperature reaches 600°C, the safety margin is −28.6 MPa, and the structure is in a failure state. Therefore, in consideration of safety, the casting crane should try to avoid the radiation effect of high temperature on the structure so as to improve the safety margin of the crane.

5. Conclusion

(1) The elastic modulus values of Q355 steel at 20°C, 100°C, 200°C, 300°C, 400°C, and 600°C were measured using a metal elastic modulus test bed. The constitutive equation for the elastic modulus at different temperatures was obtained by a polynomial fitting method, which provided a theoretical basis for analyzing the influence of temperature on crane beam vibration.

(2) The vibration model of a flexible beam-cabin-trolley-crane system based on temperature was established, and the dynamic characteristics of the beam at different temperatures were analyzed. With increasing temperature, the maximum midspan displacement of the main beam increased gradually. The midspan deflection of the main beam increased by 14.3%, 21.4%, and 57.1% at 300°C, 400°C, and 600°C, respectively.

(3) The dynamic characteristics of the cabin during trolley operation at different temperatures were analyzed. Cabin vibrational displacement increased with increasing temperature and increased by 32.5% at 600°C. However, the influence of temperature on cabin vibrational acceleration is not significant.

(4) When the crane runs at full load, the increase of midspan displacement may directly cause beam deformation to exceed the maximum allowable displacement of the crane, which poses a major threat to humans and property. Therefore, the influence of temperature on the dynamic characteristics of the girder must be considered during the design stage of casting cranes.

(5) In a certain temperature range, the yield strength and tensile strength of metal structures decrease with increasing temperature, and the safety margin of crane metal structures decreases with increasing temperature. Therefore, in order to increasing the safety margin of structure, a layer of insulation board made of asbestos mesh should be applied at the bottom of the main beam, which effectively prevents the partial radiation of temperature field to the main beam.

Data Availability

The data used to support the findings of this study are included within the article.

Conflicts of Interest

The authors declare no conflicts of interest.

Acknowledgments

This work was sponsored by the Fund for Shanxi "1331 Project" Key Subject Construction, Shanxi Science and Technology Platform Project (201805D121005), Shanxi Province Science and Technology Major Project (20181102002), Taiyuan University of Science and Technology Scientific Research Initial Funding (20182037), Doctor Excellent Award Fund for work in Shanxi (20192018), Scientific and Technological Innovation Programs of Higher Education Institutions in Shanxi (2019L0649), and Applied Basic Research Project of Shanxi Province(201901D211288).

References

[1] N. Sun, Y. Fang, H. Chen, and B. He, "Adaptive antiswing control for cranes in the presence of rail length constraints and uncertainties," *Nonlinear Dynamics*, vol. 81, no. 1-2, pp. 41–51, 2015.

[2] Z. Masoud, K. Alhazza, E. Abu-Nada, and M. Majeed, "A hybrid command-shaper for double-pendulum overhead cranes," *Journal of Vibration and Control*, vol. 20, no. 1, pp. 24–37, 2014.

[3] W. Blajer and K. Kołodziejczyk, "Motion planning and control of gantry cranes in cluttered work environment," *IET Control Theory & Applications*, vol. 1, no. 5, pp. 1370–1379, 2007.

[4] B. R. Kirby and R. R. Preston, "High temperature properties of hot-rolled, structural steels for use in fire engineering design studies," *Fire Safety Journal*, vol. 13, no. 1, pp. 27–37, 1988.

[5] J. Chen and B. Young, "Experimental investigation of cold-formed steel material at elevated temperatures," *Thin-Walled Structures*, vol. 45, no. 1, pp. 96–110, 2007.

[6] V. Kodur, M. Dwaikat, and R. Fike, "High-temperature properties of steel for fire resistance modeling of structures," *Journal of Materials in Civil Engineering*, vol. 22, no. 5, pp. 423–434, 2010.

[7] Z. D. Lu and B. L. Zhu, "Fire response analysis of reinforced concrete frames," *China Civil Engineering Journal*, vol. 28, no. 6, pp. 18–27, 1995, in Chinese.

[8] T. G. Lv, "Experimental study on strength and deformation of steel bar at elevated temperatures," Master thesis, Tsinghua University, Beijing, China, 1996.

[9] W. Tan, "Experiments and research of steel material properties at elevated temperature," *Industrial Construction*, vol. 30, no. 10, pp. 61–63, 2000, in Chinese.

[10] X. Qiang, F. S. K. Bijlaard, and H. Kolstein, "Post-fire mechanical properties of high strength structural steels S460 and S690," *Engineering Structures*, vol. 35, pp. 1–10, 2012.

[11] W. Wang, T. Liu, and J. Liu, "Experimental study on post-fire mechanical properties of high strength Q460 steel," *Journal of Constructional Steel Research*, vol. 114, pp. 100–109, 2015.

[12] European Committee for Standardization, *EN 1993-1-2, Eurocode 3: Design of Steel Structures-Part 1-2: General Rules-Structural Fire Design*, CEN, Brussels, Belgium, 2005.

[13] Standards Australia, *AS4100: Steel Structures*, SA, Sydney, Australia, 1990.

[14] ANSI/AISC 360-05, *Specification for Structural Steel Buildings*, American Institute of Steel Construction, Inc., Chicago, IL, USA, 2005.

[15] BS 5950-1:2000, *Structural Use of Steelwork in Building, Code of Practice for Design, Rolled and Welded Sections*, BSI, London, UK, 2008.

[16] GB 51249-2017, *Ministry of Housing and Urban-Rural Development of the People's Republic of China, Code for Fire Safety of Steel Structures in Buildings*, China Planning Press, Beijing, China, 2017.

[17] J. Huang, Z. Liang, and Q. Zang, "Dynamics and swing control of double-pendulum bridge cranes with distributed-mass beams," *Mechanical Systems and Signal Processing*, vol. 54-55, pp. 357–366, 2015.

[18] Z. N. Masoud and A. H. Nayfeh, "Sway reduction on container cranes using delayed feedback controller," *Nonlinear Dynamics*, vol. 34, no. 3-4, pp. 347–358, 2003.

[19] L. Frýba, *Vibration of Solids and Structures under Moving Loads*, Thomas Telford, London, UK, 1999.

[20] M. A. Foda and Z. Abduljabbar, "A dynamic green function formulation for the response of a beam structure to a moving mass," *Journal of Sound and Vibration*, vol. 210, no. 3, Article ID 051009, pp. 295–306, 1998.

[21] K. Kiani, A. Nikkhoo, and B. Mehri, "Parametric analyses of multispan viscoelastic shear deformable beams under excitation of a moving mass," *Journal of Vibration and Acoustics*, vol. 131, no. 5, pp. 1–12, 2009.

[22] K. Kiani, A. Nikkhoo, and B. Mehri, "Assessing dynamic response of multispan viscoelastic thin beams under a moving mass via generalized moving least square method," *Acta Mechanica Sinica*, vol. 26, no. 5, pp. 721–733, 2010.

[23] K. Kiani and A. Nikkhoo, "On the limitations of linear beams for the problems of moving mass-beam interaction using a meshfree method," *Acta Mechanica Sinica*, vol. 28, no. 1, pp. 164–179, 2012.

[24] International Organization of Standardization, *Metallic Materials-Tensile Testing-Part 1: Method of Test at Room Temperature ISO 6892-1*, ISO, Geneva, Switzerland, 2009.

[25] International Organization of Standardization, *Metallic Materials-Tensile Testing at Elevated Temperature ISO 783-1*, ISO, Geneva, Switzerland, 1999.

[26] G. Yuan, Q. Shu, Z. Huang, and Q. Li, "An experimental investigation of properties of Q345 steel pipe at elevated temperatures," *Journal of Constructional Steel Research*, vol. 118, pp. 41–48, 2016.

[27] European Convention for Constructional Steelwork, *European Recommendations for the Fire Safety of Steel Structures, Calculation of the Fire Resistance*, Elsevier Scientific Pub. Co., Amsterdam, Netherlands, 1983.

[28] N. S. Trahair, *The Behaviour and Design of Steel Structures*, Chapman & Hall, London, UK, 1988.

[29] Y. Xin, G. Xu, N. Su, and Q. Dong, "Nonlinear vibration of ladle crane due to a moving trolley," *Mathematical Problems in Engineering*, vol. 2018, no. 4, Article ID 5756180, 14 pages, 2018.

[30] G. T. Michaltsos, "Dynamic behaviour of a single-span beam subjected to loads moving with variable speeds," *Journal of Sound and Vibration*, vol. 258, no. 2, pp. 359–372, 2002.

[31] D. C. D. Oguamanam, J. S. Hansen, and G. R. Heppler, "Dynamics of a three-dimensional overhead crane system," *Journal of Sound and Vibration*, vol. 242, no. 3, pp. 411–426, 2001.

[32] S. Park and Y. Youm, "Motion of a moving elastic beam carrying a moving mass-analysis and experimental verification," *Journal of Sound and Vibration*, vol. 240, no. 1, pp. 131–157, 2001.

[33] H.-Y. Lin, "Dynamic analysis of a multi-span uniform beam carrying a number of various concentrated elements," *Journal of Sound and Vibration*, vol. 309, no. 1-2, pp. 262–275, 2008.

[34] W. Xie, J. Huang, J. Zhou et al., "Vibration analysis of a suspension weight-bridge crane coupled system," *Journal of Vibration and Shock*, vol. 34, no. 15, pp. 127–132, 2015.

[35] H. Liu, W. Cheng, and Y. Li, "Dynamic responses of an overhead crane's beam subjected to a moving trolley with a pendulum payload," *Shock and Vibration*, vol. 2019, Article ID 1291652, 14 pages, 2019.

[36] B. Zheng, X. Gao, and C. Zhang, "Radial integration BEM for vibration analysis of two- and three-dimensional elasticity structures," *Applied Mathematics and Computation*, vol. 277, pp. 111–126, 2016.

[37] Z. Hu, C. Su, T. Chen, and H. Ma, "An explicit time-domain approach for sensitivity analysis of non-stationary random vibration problems," *Journal of Sound and Vibration*, vol. 382, pp. 122–139, 2016.

[38] E. Esmailzadeh and M. Ghorashi, "Vibration analysis of beams traversed by uniform partially distributed moving masses," *Journal of Sound and Vibration*, vol. 184, no. 1, pp. 9–17, 1995.

[39] J. J. Wu, "Dynamic responses of a three-dimensional framework due to a moving carriage hoisting a swinging object," *International Journal for Numerical Methods in Engineering*, vol. 59, no. 13, pp. 1679–1702, 2004.

[40] GB/T 3811-2008, *Design Rules for Cranes*, Standards Press of China, Beijing, China, 2008.

[41] International Organization of Standardization, *Cranes-Design Principles for Loads and Load Combinations-Part 1: General First Ed ISO8686-1*, Geneva, Switzerland, 2012.

[42] D. Younesian, E. Ghafoori, and M. Sadeghpour, "Nonlinear vibration of a three-dimensional moving gantry crane subjected to a travelling trolley hoisting a swinging object," *Transactions of the Canadian Society for Mechanical Engineering*, vol. 34, no. 3-4, pp. 333–350, 2010.

[43] G. Xu, *Machinery and Equipment Metal Structure Design*, Mechanical Industry Press, Beijing, China, 2018.

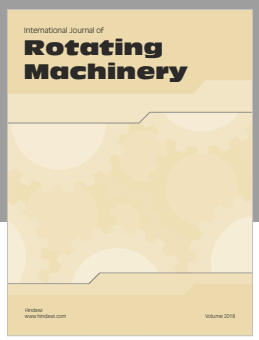

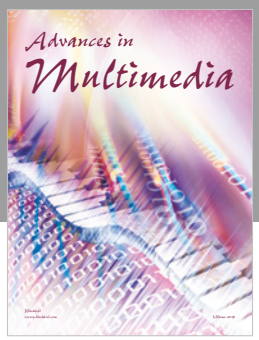

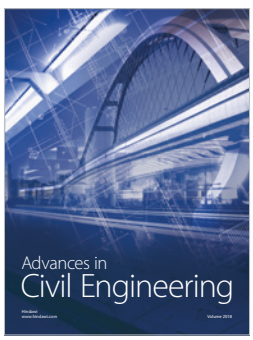

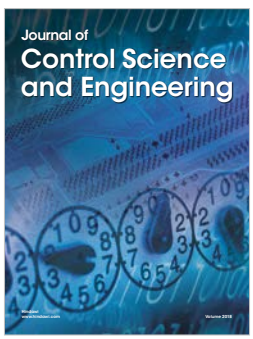

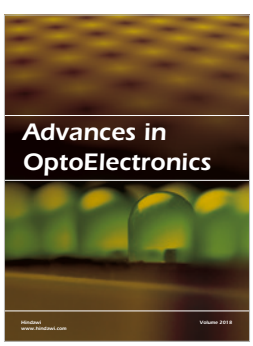

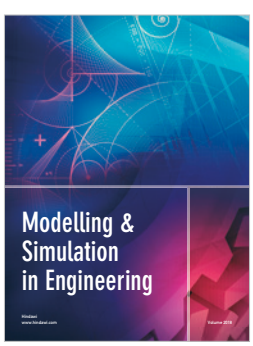

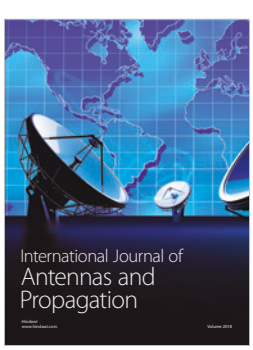

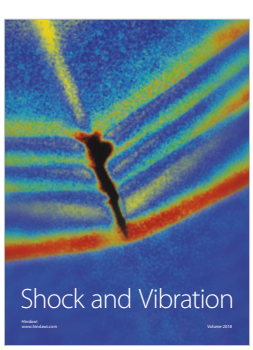

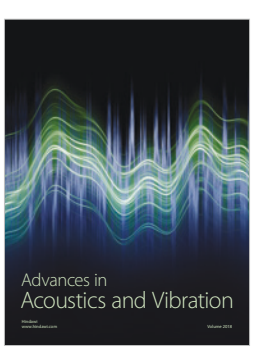

Hindawi

Submit your manuscripts at
www.hindawi.com